Journal of Power Sources 218 (2012) 320–330

Contents lists available at SciVerse ScienceDirect

Journal of Power Sources

journal homepage: www.elsevier.com/locate/jpowsour

# Direct synthesis of palladium nanoparticles on $Mn_3O_4$ modified multi-walled carbon nanotubes: A highly active catalyst for methanol electro-oxidation in alkaline media

Yanchun Zhao [a,*], Sulian Nie [a], Huaiwen Wang [b], Jianniao Tian [a], Zhen Ning [a], Xiaoxiao Li [a]

[a] Key Laboratory for the Chemistry and Molecular Engineering of Medicinal Resources (Ministry of Education of China), College of Chemistry and Chemical Engineering, Guangxi Normal University, Guilin 541004, PR China
[b] Laboratory for Molecular Biology and Cytometry Research, The University of Oklahoma Health Sciences Center, Oklahoma City, OK 73104, USA

## HIGHLIGHTS

- Excellent electrocatalytic activity and anti-$CO_{ads}$ poisoned ability toward methanol electro-oxidation in alkaline media.
- Increased catalytic activity is related to the $Mn_3O_4$ nanoparticles on the catalyst surface.
- $E_a$ values demonstrated Pd–$Mn_3O_4$/MWCNT catalyst is more accessible reaction toward methanol electro-oxidation.

## ARTICLE INFO

*Article history:*
Received 8 March 2012
Received in revised form
21 May 2012
Accepted 4 July 2012
Available online 14 July 2012

*Keywords:*
Multi-walled carbon nanotubes
Trimanganese tetraoxide
Palladium nanoparticles
Electro-oxidation
Alkaline direct methanol fuel cells

## ABSTRACT

A facile preparation route for Pd electrocatalyst (Pd–$Mn_3O_4$/MWCNTs) composed of ~3.5 nm Pd nanoparticles homogeneously anchored on $Mn_3O_4$ modified multi-walled carbon nanotubes ($Mn_3O_4$/MWCNTs) is reported. The morphology, component and crystallinity of the catalyst were characterized by means of different techniques. The electrochemical behavior of the Pd–$Mn_3O_4$/MWCNT composites was examined by cyclic voltammetry toward methanol electro-oxidation in alkaline media. Pd nanoparticles binding on the surface of the $Mn_3O_4$/MWCNTs exhibited improved electrocatalytic activity and anti-$CO_{ads}$ species poisoned ability compared to Pd/MWCNTs and Pd/XC-72 (Pd/commercial Vulcan XC-72 carbon black). This improved performance of the as-prepared electrocatalyst is attributed to the synergistic effect of $Mn_3O_4$ nanoparticles and MWCNTs.



## 1. Introduction

Since the electrical, optical, and magnetic properties of nanoparticles are mainly decided by their dimension [1], the fabrication of uniform-sized nanoparticles is of key importance for their fundamental scientific and technological applications. Nowadays, manganese oxides (MnOx) have attracted considerable interest due to their applications in catalysts, ion-exchanging materials, electrochemical materials, high-density magnetic storage media, solar energy transformation and molecular adsorption [2–5]. Among the series of MnOx (MnO, $Mn_2O_3$ and $Mn_3O_4$), trimanganese tetraoxide ($Mn_3O_4$) is reputed to be an active catalyst in some oxidation or reduction reactions such as the oxidation of methane and carbon monoxide [6] and the selective reduction of nitrobenzene [7]. Compared to other oxides, such as $CeO_2$ or $Co_3O_4$, MnOx have two crucial factors attracting investigators for commercialization: (i) The relative abundance, low cost and environmental benignity of manganese (Mn) [8], lead to MnOx, especially $Mn_3O_4$, an anode material for direct alcohol fuel cells, (ii) MnOx are effective promoter or appropriate supporting materials for fabricating prominent Pd-based electrocatalysts toward alcohols or methanol oxidation [9,10] due to the exist of MnOOH species which generated in alkaline reaction medium [11–14]. For example, Shen and Xu reported that the Pd electrocatalysts supported on oxide/C materials showed much higher catalytic activity and stability than those of Pd/C or Pt/C electrocatalyst in alcohol oxidation [9,15]. The specific reaction mechanisms were described as follow: In alcohols oxidation reaction, the oxygen-containing species ($OH_{ad}$) are formed first on the surface of oxides, as mentioned above as MnOOH species, which subsequently react with CO-like

* Corresponding author. Tel.: +86 773 5846279; fax: +86 773 2120958.
*E-mail address:* yanchunzh@yahoo.cn (Y. Zhao).

0378-7753/$ – see front matter © 2012 Elsevier B.V. All rights reserved.
http://dx.doi.org/10.1016/j.jpowsour.2012.07.012

intermediate species on Pd to produce $CO_2$ or other insoluble products and release the active sites for further electrochemical reaction [16]. Xu et al. and Zhang et al. successfully deposited Pd nanoparticles on tube-like transition metal oxides (β-$MnO_2$, $VO_x$), and discovered the products are remarkable catalysts for methanol oxidation [10,17]. Although the exact mechanisms are still unclear, the significant effects of transition metal oxides in the methanol oxidation have been commonly recognized. Moreover, owing to its low cost and relative high electrocatalytic activity, MnOx have been known to be one of the most promising catalysts for oxygen reduction [18].

Recently, many methods have been reported to prepare $Mn_3O_4$, such as manganese salt precursors calcination [19], chemical bath deposition [20], sol–gel technique [21] and the co-precipitation method [22] etc. Multifarious nanostructured $Mn_3O_4$ including dendritic clusters, nanowires, nanotubes, nanobelts, nanocrystals with different shapes, and nanoflowers, have also been synthesized [23,24]. However, considering the $Mn_3O_4$ preparation is still complex and costly, it is necessary to develop a simple method to synthesize small-sizes nano-$Mn_3O_4$. There are two important factors affecting the behaviors of MnOx: surface area of manganese oxide and the electrical conductivity [25]. Therefore, a material with high surface area and good conductivity in combination with MnOx as the support would be the key for developing cheap, efficient electrocatalysts. In this paper, we found a novel and facile one-step method to prepare uniform $Mn_3O_4$ nanoparticles, which deposited on the surface of multi-walled carbon nanotubes (MWCNTs) evenly. This method was performed with a simple reduction process at room temperature without extortionate material or rigorous condition. MWCNTs are considered as good catalyst supports for direct methanol fuel cells. The substitution of carbon black particles with multiwalled CNTs as the catalyst support material improves the performance in DMFCs [26]. Due to more regular pore structures, conductive paths and faster rates of electron transfer of MWCNTs [27,28], the poor electric conduction of single $Mn_3O_4$ was greatly improved. Then, $Mn_3O_4$/MWCNTs were used as supports to synthesize Pd-based (Pd–$Mn_3O_4$/MWCNT) catalysts by an incipient wet method strategy. Pd nanoparticles on $Mn_3O_4$/MWCNTs have higher electrochemical surface area and better activity than that of Pd/MWCNTs and Pd/XC-72 for electrochemical oxidation of methanol in alkaline solution. Furthermore, the lower activation energies ($E_a$) values of the as-prepared catalyst suggest the possibility for applications of Pd–$Mn_3O_4$/MWCNTs in alkaline direct methanol fuel cells.

## 2. Experimental

### 2.1. Materials

All chemical reagents used in this experiment were of analytical grade. Sulfuric acid, nitric acid, hydrochloric acid, ethanol, methanol, NaOH, $H_2PdCl_4$, $KMnO_4$, $NaBH_4$ and polyethlyleneglycol 20,000 (PEG 20000) were procured commercially and used without further purification. The raw MWCNTs were purchased from Shenzhen Nanotechnologies Port Co. Ltd. (Shenzhen, China) with the diameter of 40–60 nm, length of 5–15 μm, and purity of 98%. Nafion (perfluorosulfonic acid-PTFE copolymer) was purchased from Alfa Aesar (A Johnson Matthey Company) with the concentration of 5% w/w solution.

### 2.2. Preparation of $Mn_3O_4$/MWCNTs

Raw-MWCNTs were refluxed in a concentrated $H_2SO_4$–$HNO_3$ mixture (8.0 M for each acid) at a bath temperature of 80 °C with duration of 2 h to remove the impurities. The acid-treated MWCNTs (AO-MWCNTs) were washed for several times with deionized water and dried in a vacuum oven at 70 °C for 12 h for further use.

For preparing the $Mn_3O_4$/MWCNT composites, the AO-MWCNTs, hydrochloric acid (HCl) and potassium permanganate ($KMnO_4$) were used as the starting material, PEG 20000 as the surfactant and reducing agent. A typical synthesis route was as follows: 5 mL of 0.1 M $KMnO_4$ and 2.5 mL of 50 g $L^{-1}$ PEG 20000 was mixed in 100 mL beaker, stirred for 30 min. 30 mg AO-MWCNTs and 10 mL of $H_2O$ was dispersed in 50 mL beaker after 30 min sonication and this suspension was added into the above solution with continuous stirring for 2 h. Then 1.0 M hydrochloric acid was added to the solution until its pH dropped to about 2.0, and then stirred about 2 h at room temperature until the color of the $KMnO_4$ faded. Finally, the resulting product was centrifuged, washed with deionized water and ethanol respectively, dried overnight at 70 °C to obtain high purified $Mn_3O_4$/MWCNTs.

### 2.3. Preparation of Pd–$Mn_3O_4$/MWCNTs catalyst

Pd–$Mn_3O_4$/MWCNTs (20 wt.% metal content) nano-sized catalysts were synthesized using $NaBH_4$ as reducing agent by wet impregnation method: 20 mg of $Mn_3O_4$/MWCNTs powder was dispersed in 20 mL ethanol/water (1:1, v/v ratio) solution in 100 mL beaker, mixed with 9.4 mL of 5 mM $H_2PdCl_4$ solution and stirred for 10 h. A freshly prepared solution of 50 mg $NaBH_4$ in 10 mL water was added dropwise into the above solution under vigorous stirring. After stirred for an additional 2 h, the black solid was centrifuged and washed with deionized water for several times, and then dried overnight in oven at 70 °C. For comparison, Pd nanoparticles supported on MWCNTs and Vulcan XC-72 catalysts were also obtained by the same process. The $Mn_3O_4$ content of prepared Pd–$Mn_3O_4$/MWCNTs was 40 wt. % and the palladium loading of every catalysts was 20 wt. %.

### 2.4. Characterization

Morphology, component and microstructure of the synthesized materials were observed with scanning electron microscopy (SEM) (FEI Quanta 200 FEG, Holand), EDS (FEI Quanta 200 FEG, Holand) and high-resolution transmission electron microscopy (HRTEM) (JEM-2100F, Japan). The X-ray powder diffraction (XRD) patterns were collected on a Rigaku D/MAX 2500v/pc (Japan) diffractometer with Cu Ka radiation. The electronic structure of the catalysts was determined by X-ray photoelectron spectroscopy (XPS) (JPS-9010TR, Japan) with Mg Ka radiation. The microstructure of as-prepared $Mn_3O_4$/MWCNTs was also characterized by means of Raman spectroscopic analysis. All electrochemical measurements were carried out on a CHI660C electrochemical working station using a conventional three electrode cell with a saturated calomel electrode (SCE) and a platinum sheet as the reference and counter electrodes, respectively. A glassy carbon electrode (GC, $Ø = 3$ mm) was used as the working electrode, on which a thin layer of Nafion-impregnated catalyst was cast. The electro-oxidation activity of the as-prepared catalyst was measured by cyclic voltammetry (CV) measurements in a 0.5 M NaOH solution containing 1.0 M methanol with the potential cycled between −1.0 and 0.5 V and a scan rate of 50 mV $s^{-1}$ at 25 °C.

## 3. Results and discussion

### 3.1. The mechanism of the Pd–$Mn_3O_4$/MWCNTs formation

The schematic of preparation mechanism of Pd–$Mn_3O_4$/MWCNTs is shown in Fig. 1. After the acid-treatment, MWCNTs with oxygenous functional groups, such as carbonyl or carboxyl

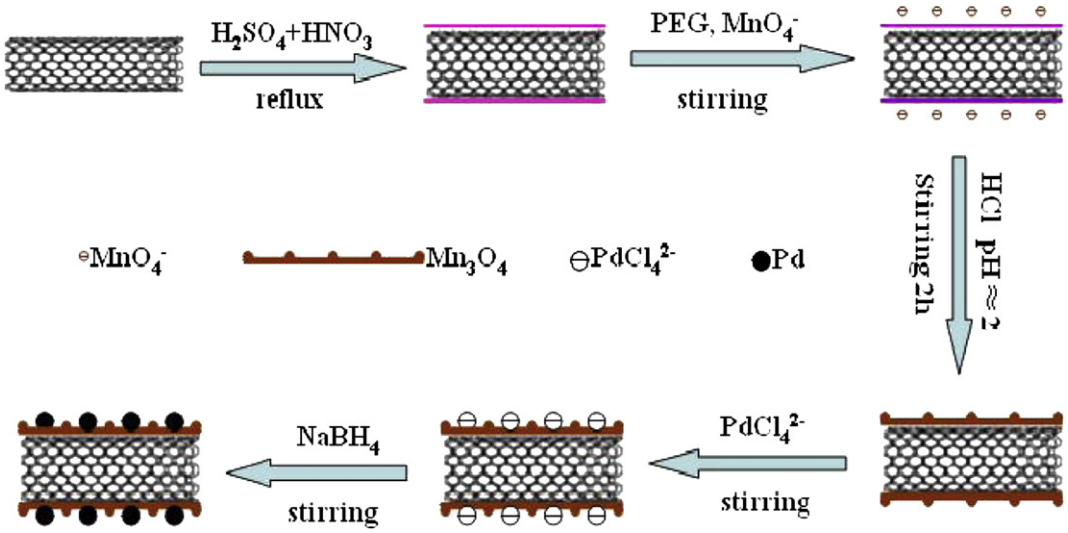


**Fig. 1.** The preparation mechanism of Pd–$Mn_3O_4$/MWCNT composites.

groups, were obtained. These oxidation points and defects on MWCNTs offer binding sites for $Mn_3O_4$ [27]. Then $Mn_3O_4$ layer wrapped on the surface of MWCNTs in the presence of PEG 20000 acting as reducing agent and surface active agent, $KMnO_4$ serving as $Mn_3O_4$ precursor, and HCl for providing an acid medium and expediting the reaction process. After the deposition of $Mn_3O_4$, the surface on the MWCNTs became rougher and produced more active area and defect sites for Pd dispersing. In the presence of $NaBH_4$ and

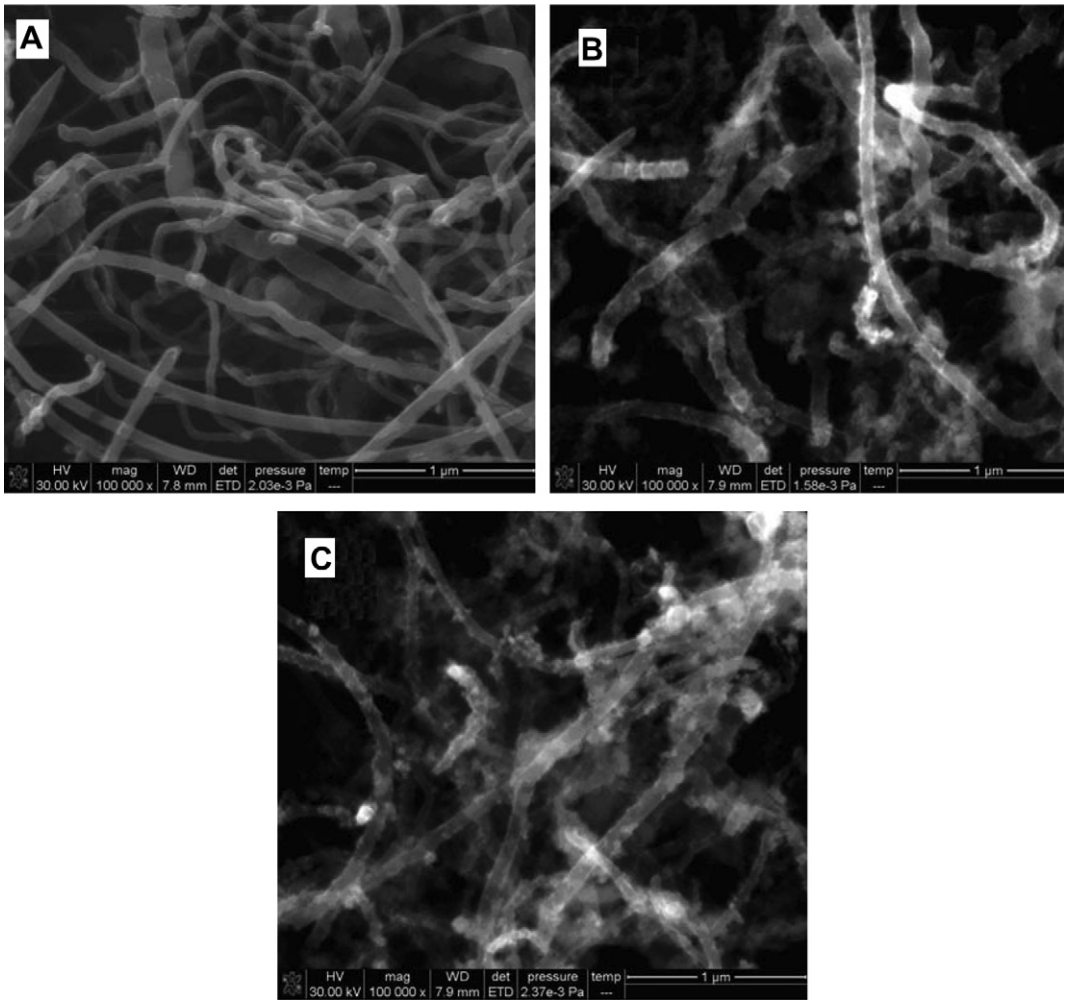


**Fig. 2.** SEM images of AO-MWCNTs (A), $Mn_3O_4$/MWCNTs (B) and Pd–$Mn_3O_4$/MWCNTs (C).

$H_2PdCl_4$ with continuous stirring, monodispersed Pd nanoparticles binding on $Mn_3O_4$/MWCNT composites were obtained.

### 3.2. Structural and compositional analysis

The SEM images of AO-MWCNT (A), $Mn_3O_4$/MWCNTs (B) and Pd–$Mn_3O_4$/MWCNT composites (C) are shown in Fig. 2. The AO-MWCNTs are tangled ropes with smooth surfaces in the SEM image (Fig. 2A). The surface of $Mn_3O_4$/MWCNTs in SEM (Fig. 2B) is relative rough, which is result of $Mn_3O_4$ layer wrapping the sidewalls of MWCNTs. It can be also seen that more metal nanoparticles exhibit well-uniform dispersion and size distribution on the surface of $Mn_3O_4$/MWCNTs (Fig. 2C). The chemical composition of $Mn_3O_4$/MWCNTs and Pd–$Mn_3O_4$/MWCNTs determined using energy-dispersive X-ray spectroscopy (EDS) analysis are shown in Fig. 3A and Fig. 3B, respectively. The peaks of Mn, C and O are found on $Mn_3O_4$/MWCNTs, and the peaks of Pd, Mn, C and O are observed on Pd–$Mn_3O_4$/MWCNTs. Additionally, the mapped SEM micrographs show the elements (C, O, Mn, Pd) are well-dispersed in the Pd–$Mn_3O_4$/MWCNT catalysts (Fig. 4).

Fig. 5 shows representative TEM images of $Mn_3O_4$/MWCNT composites (A), Pd–$Mn_3O_4$/MWCNT composites (B), and the HRTEM image of Pd–$Mn_3O_4$/MWCNT composites (C), respectively. As shown in Fig. 5A, most of $Mn_3O_4$ particles were floc and uniformly covered the surface of the MWCNTs. It should be pointed out that the interaction between nanoparticles and MWCNTs was strong because the nanoparticles could not be removed by thorough wash and severe agitation. Comparing TEM images of $Mn_3O_4$/MWCNTs (A) with Pd–$Mn_3O_4$/MWCNTs (B), Pd nanoparticles with diameters in the range from 3 to 5 nm are well dispersed onto the external walls of $Mn_3O_4$/MWCNTs, which is agreement with the XRD analysis (inset in Fig. 7A). HRTEM of the prepared Pd–$Mn_3O_4$/MWCNT shows two dominant crystal lattice stripes (Fig. 5C). The smaller one of $d$ 0.225 nm in sample can be attributed to Pd metal ($d$ 0.2246 nm, JCPDS card No. 46-1043), and the other one of $d$ spacing is 0.49 nm, which corresponds to that of the {101} lattice planes of $Mn_3O_4$ ($d$ 0.4924 nm, JCPDS card No. 24-0734). This results implying the existence of Pd and $Mn_3O_4$ nanoparticles on the surface of the MWCNT support.

XPS was used to determine the surface oxidation states of the species in composites. Fig. 6A shows the full-scale XPS spectrum for Pd–$Mn_3O_4$/MWCNT (a) and $Mn_3O_4$/MWCNT (b) composites. Fig. 6B displays the XPS spectra for the Mn $2p_{3/2}$ and Mn $2p_{1/2}$ of the Pd–$Mn_3O_4$/MWCNT composites and Fig. 6C presents the XPS spectra of Pd 3d peaks of Pd–$Mn_3O_4$/MWCNT composites, respectively. The result in Fig. 6A reveals the presence of C, O, Pd and Mn elements in the Pd–$Mn_3O_4$/MWCNT catalysts. Meanwhile, the Mn(II) and Mn(IV;) species are present in Fig. 6B. It can be viewed that Mn $2p_{3/2}$ band appeared at 641.8 eV and Mn $2p_{1/2}$ band at 653.5 eV in the sample. In addition, the observed spin-energy separation is about 11.7 eV, which is in agreement with that of $MnO_x$ reported in the literature [2,27,29,30]. In spectrum for Mn 2p, there are two pairs of peaks: one at 641.8 eV, which is in accordance with the Mn $2p_{3/2}$ of MnO and another at 642.8 eV, which could be attributed to the Mn $2p_{3/2}$ of $MnO_2$ [27,30]. Theoretical calculation demonstrates $MnO_2$ in $Mn_3O_4$ is about 40 wt% and the rest of $Mn^{2+}$ is about 60 wt% [30]. In Fig. 6B, the area ratio (i.e. molar ratio) of $Mn^{4+}$ versus $Mn^{2+}$ is approximately 1:2, which agrees well with the theoretical value. Therefore, it can be concluded that the particle modified on MWCNTs is $Mn_3O_4$. Fig. 6C shows typical Pd 3d

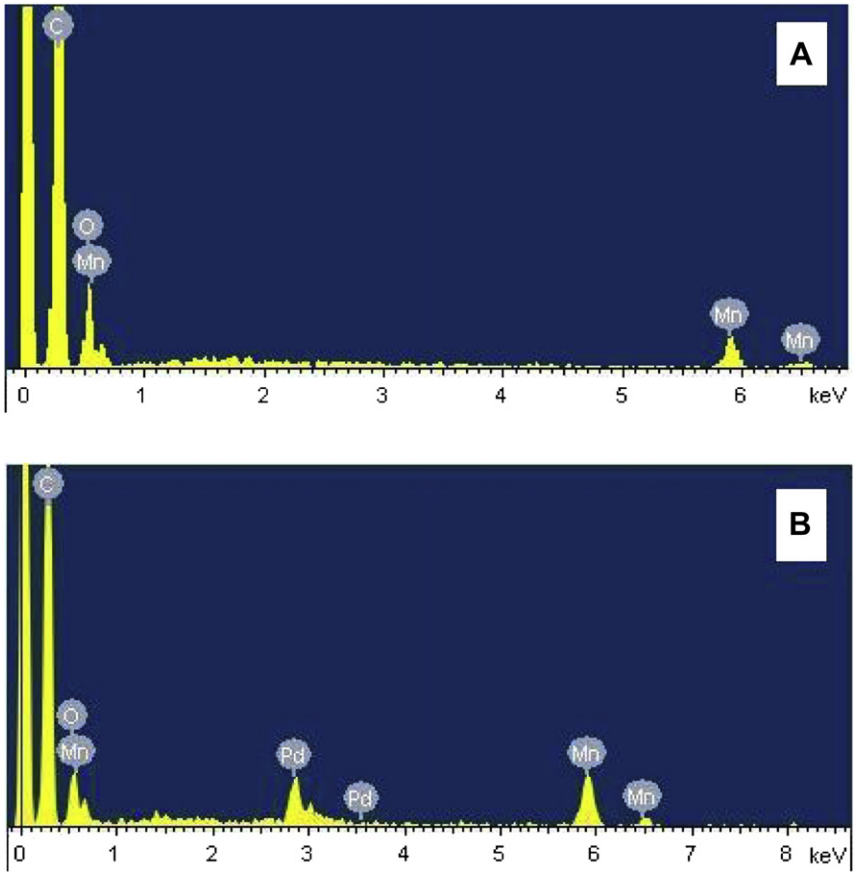


**Fig. 3.** EDS spectra of $Mn_3O_4$/MWCNT composites (A) and Pd–$Mn_3O_4$/MWCNT composites (B).

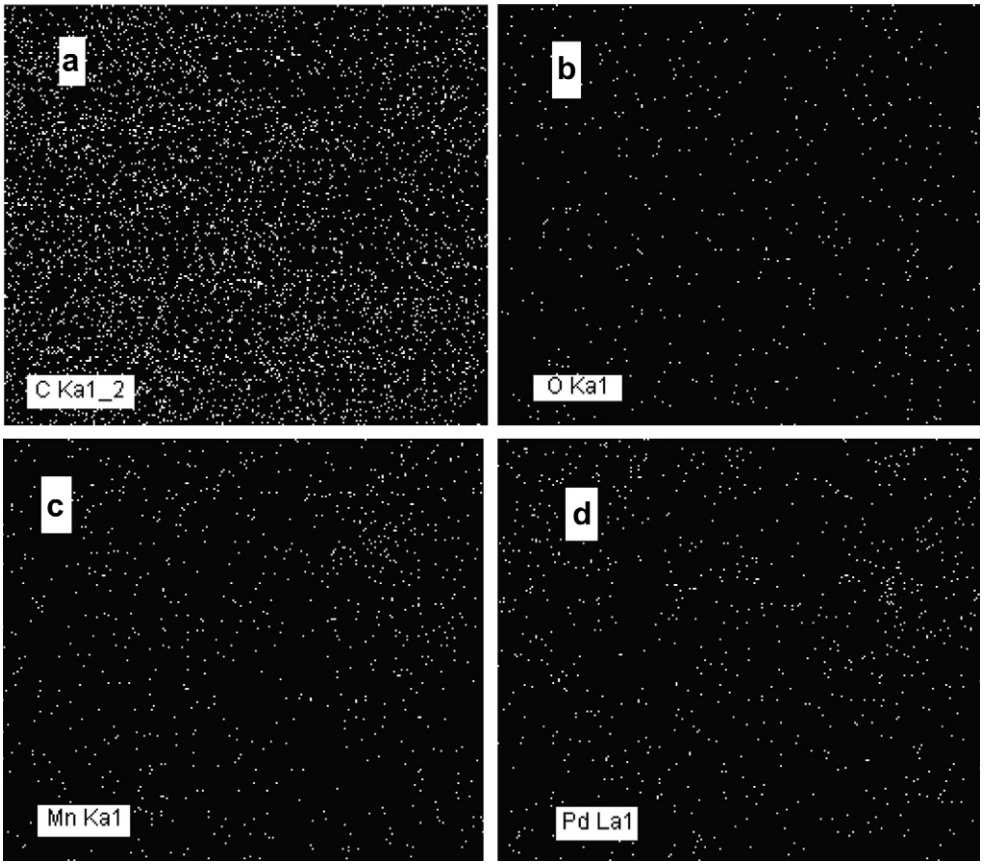


**Fig. 4.** The mapped SEM micrographs of the elements in the Pd–$Mn_3O_4$/MWCNT catalysts: (a) C, (b) O, (c) Mn, and (d) Pd.

XPS spectra of Pd–$Mn_3O_4$/MWCNT catalyst. The presence of Pd $3d_{5/2}$ and $3d_{3/2}$ peaks at binding energy of 335.77 eV and 341.15 eV, respectively, indicates that the Pd in Pd–$Mn_3O_4$/MWCNTs exists mainly in metallic form [28,31,32].

Fig. 7A shows the XRD patterns of Pd–$Mn_3O_4$/MWCNT composites, together with the Pd/MWCNT and Pd/XC-72 composites. The presence of $Mn_3O_4$ in the composites is confirmed by the characteristic diffraction peaks, which can be perfectly indexed to $Mn_3O_4$ structure (Hausmannite). The lattice constants are in good consistent with the standard values of single phase of $Mn_3O_4$ (JCPDS NO. 24-0734). No other characteristic peaks are observed, demonstrating the high purity of these samples. As displayed in Fig. 7A, the XRD pattern of Pd–$Mn_3O_4$/MWCNT composites shows the diffraction peaks at 18°, 29°, 31°, 32.4°, 36.1°, 38.1°, 44.4°, 50.8°, 58.5°, 59.9°, and 64.6°, which are attributed to the characteristic peaks of $Mn_3O_4$ [18], corresponding to crystalline planes of $Mn_3O_4$ (101) (112) (200) (103) (211) (004) (220) (105) (321) (224) and (314), respectively. The average $Mn_3O_4$ particle size in the Pd–$Mn_3O_4$/MWCNT composites is estimated to be 7.6 nm on the basis of the $Mn_3O_4$ (211) peak by Scherrer equation [33]: $d = 0.9\lambda/\beta cos\theta$ (where $\lambda$ is the wavelength of the X-rays used (1.54, 056 Å), $\beta$ is the width of the diffraction peak at half height in radians, and $\theta$ is the angle at the position of the peak maximum). The broad peaks at $2\theta = 26°$ and 54.35° are associated with the (002) and (004) planes of the graphite-like structure of the multi-walled carbon nanotubes [34,35]. The diffraction peaks at $2\theta = 40.1°$, 46.6°, 68.1° and 82.1° are assigned to the (111) (200) (220) and (311) crystalline planes of Pd face-centered cubic (fcc) structure [28,36], respectively. The Pd (111) peaks are used to calculate the particle size of Pd according to Scherrer equation. The mean Pd nanoparticles size of Pd/MWCNT and Pd–$Mn_3O_4$/MWCNT electrocatalysts are estimated to be 6.2 and 3.4 nm, respectively. The results indicate that noble metal particles are dispersed better on $Mn_3O_4$/MWCNTs than on MWCNTs. Comparing with the XRD patterns of Pd/MWCNTs and Pd/XC-72, there is no visible shift in the diffraction peaks of noble metal in Pd–$Mn_3O_4$/MWCNTs, indicating that the addition of oxide has no obvious effect on the crystalline lattice of noble metal [28].

In addition, the Raman spectra were also used to investigate the surface structure of AO-MWCNTs (a), raw MWCNTs (b), and $Mn_3O_4$-MWCNTs (c). The results are shown in Fig. 7B. $Mn_3O_4$-MWCNTs (c) have three different bands between 300 $cm^{-1}$–700 $cm^{-1}$, which can be used to identify the microstructure information on the molecular scale of as-prepared $Mn_3O_4$ nanoparticles [37,38]. There are no other diffraction peaks corresponding to impurities, suggesting its good crystalline quality. From the Raman spectrum, we can clearly find three main Raman peaks corresponding to crystalline hausmannite structure, especially the most important peak at 650.95 $cm^{-1}$ [39]. Moreover, the D and G bands at ~1345 and ~1570 $cm^{-1}$, respectively, reflect the structure of sp3 and sp2 hybridized carbon atom [40], indicating the defects/disorder-induced modes and in-plane vibrations of the graphitic wall [41]. Therefore, the degree of the graphitization of MWCNTs can be quantified by the intensity ratio of D to G bands. The peak intensity ratios ($I_D/I_G$) are 0.66, 0.63, and 0.85 for $Mn_3O_4$-MWCNT, raw MWCNT, and AO-MWCNT samples, respectively. The largest $I_D/I_G$ ratio of the AO-MWCNT sample implies that AO-MWCNTs contain more amorphous carbon impurities than the other two MWCNT samples [41]. This result implies that the harsh chemical acid treatment produces carboxylic acid sites on the surface, causing significant structural damage of MWCNTs. This would decrease the electrical conductivity of MWCNTs and lower the corrosion resistance [42,43]. However, the $Mn_3O_4$ functionalization method can provides highly effective

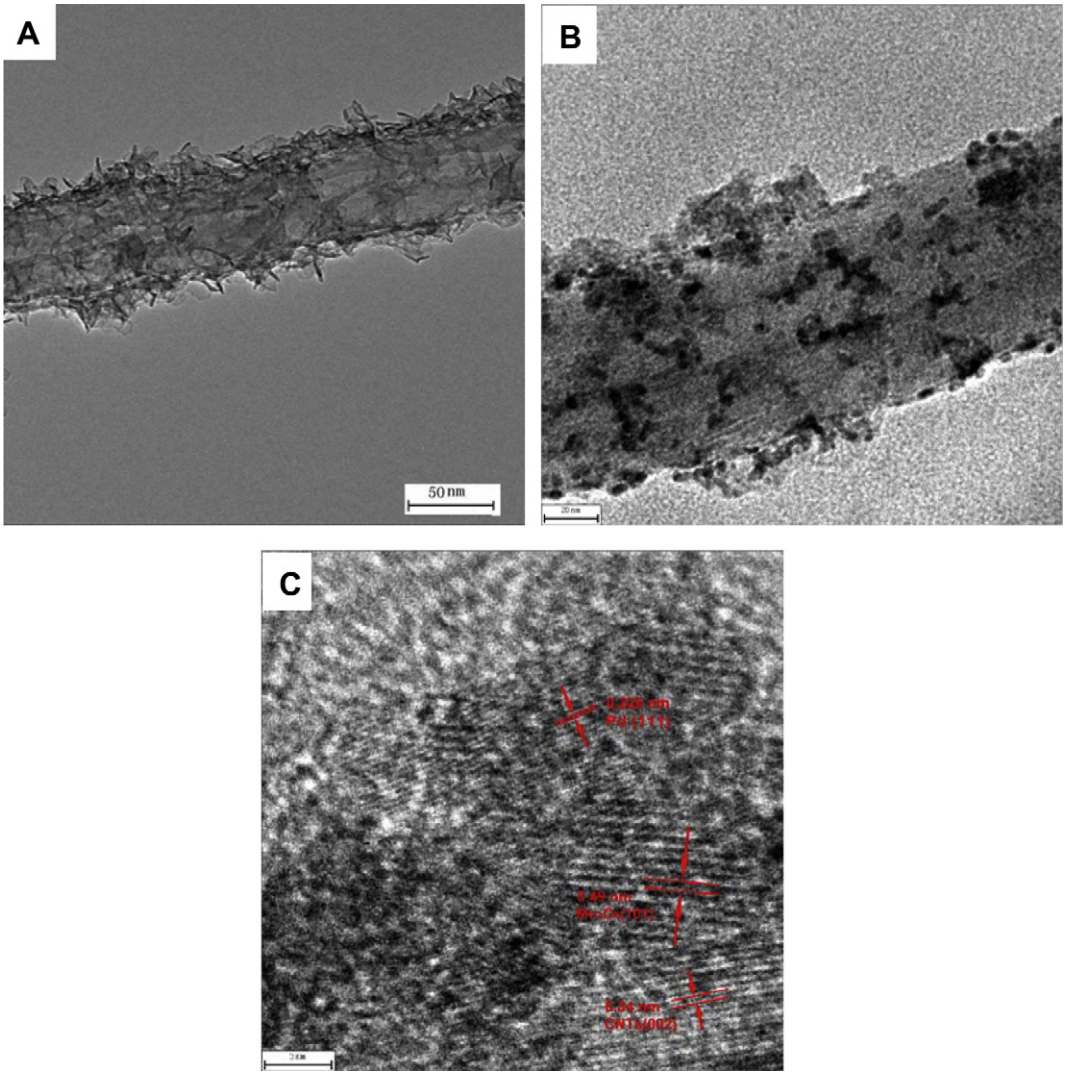


**Fig. 5.** TEM images of the $Mn_3O_4$/MWCNT composites (A), Pd–$Mn_3O_4$/MWCNT composites (B) and the HRTEM image of the Pd–$Mn_3O_4$/MWCNT composites (C).

functional groups on the surface of MWCNTs for the subsequent deposition Pd nanoparticles [44], by preferably preserving the integrity and electronic structure of carbon nanotubes.

### 3.3. The electrochemical surface area of the catalysts

The CV of the Pd–$Mn_3O_4$/MWCNT catalysts in 0.5 M NaOH at a scan rate of 50 mV $s^{-1}$ between −1.0 V and 0.5 V is shown in Fig. 8. For comparison, the CV of the Pd/MWCNT and Pd/XC-72 catalysts are also presented. It can be seen that the current peak associated with the reduction of palladium oxide in the CV obtained from the Pd–$Mn_3O_4$/MWCNT catalysts shifts to more negative potential as compared to that of the Pd/MWCNT catalysts. From the CV curves of Pd/XC-72 and Pd/MWCNTs, a flat anodic ($E \approx 0.4$ V) and a strong cathodic ($E \approx -0.45$ V) peak corresponding the formation and reduction of palladium oxide could be seen [28]. However, during the whole process, the Pd–$Mn_3O_4$/MWCNTs undergone a multi-reaction on the surface of the electrode. Peak $P_2$ and $P_5$ correspond to the redox reaction equation as follow [11]:

$$Mn_3O_4 \cdot 2H_2O + OH^- \rightleftarrows 2MnOOH + Mn(OH)_3 + e^-$$

Peak $P_3$ and $P_4$ correspond to the redox reaction equation as follow:

$$2(2MnOOH + Mn(OH)_3) + 3OH^- \rightleftarrows (6MnO_2) \cdot 5H_2O + 3H^+ + 6e^-$$

Peak $P_1$ and $P_6$ correspond to the redox reaction equation as follow:

$$Mn_3O_4 \cdot 2H_2O + 2H^+ + 2e^- \rightleftarrows 3Mn(OH)_2$$

In the low potential range, the surface is covered by $Mn_3O_4$. As the potential continue to move toward the positive direction, $Mn_3O_4$ is transformed into $Mn_2O_3$ and $MnO_2$ [11].

In addition, it is known that the activity of a catalyst is controlled by two factors, one is the catalytic properties, and the other is the geometrical properties. Therefore, the electrochemical active surface area (*ESA*) of the catalysts could be measured by determining the coulombic charge for the reduction of palladium oxide [45,46]. The *ESA* is estimated using the equation:

$$ESA = \frac{Q}{SI}$$

Where 'S' is the proportionality constant; '*l*' is the catalyst loading in 'g'. A charge value of 405 μC $cm^{-2}$ is assumed for the reduction of PdO monolayer [47]. The *ESA* values calculated are in the following

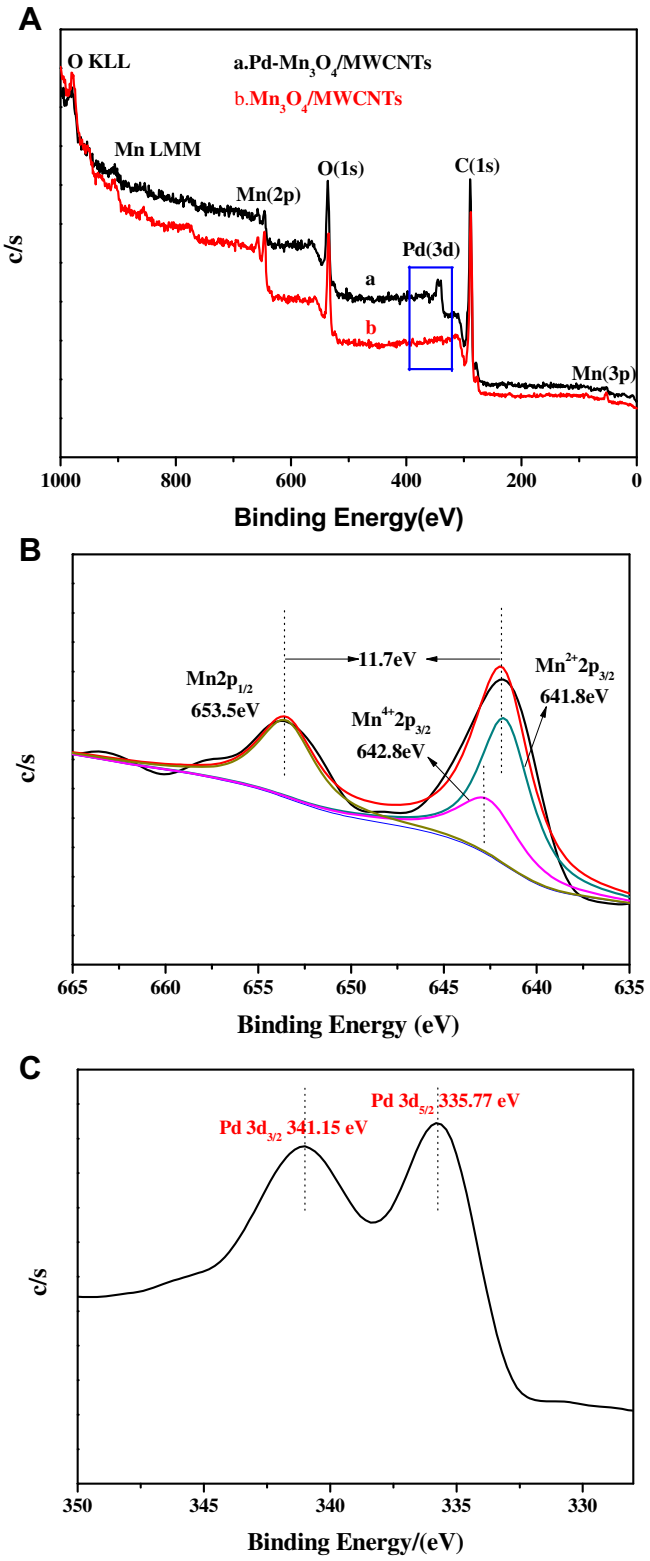


**Fig. 6.** XPS survey spectra of Pd–$Mn_3O_4$/MWCNT and $Mn_3O_4$/MWCNT composites (A); and the XPS spectrum for Mn 2p (B) and Pd 3d (C) regions of Pd–$Mn_3O_4$/MWCNT composites.

order: *ESA* (Pd–$Mn_3O_4$/MWCNTs)> *ESA* (Pd/MWCNTs)> *ESA* (Pd/XC-72).

Fig. 9 shows the CO-stripping voltammograms and the subsequent CV for the Pd/XC-72 (Fig. 9a) and Pd/MWCNT (Fig. 9b) along

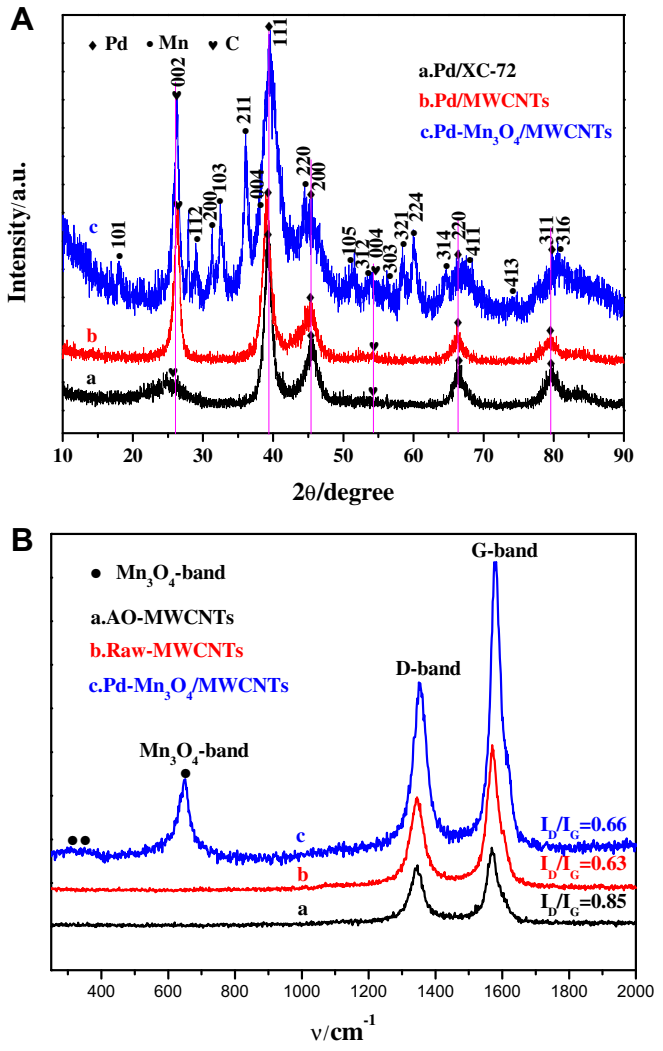


**Fig. 7.** The XRD patterns (A) of (a) Pd/XC-72, (b) Pd/MWCNT, (c) Pd–$Mn_3O_4$/MWCNT composites and Raman spectra (B) of as-prepared AO-MWCNTs (a), raw MWCNTs (b) and $Mn_3O_4$-MWCNTs (c).

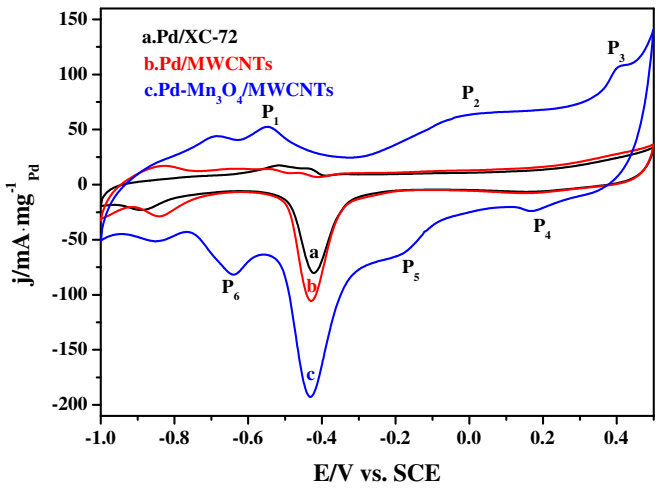


**Fig. 8.** Cyclic voltammograms of the Pd/XC-72 (a), Pd/MWCNTs (b) and Pd–$Mn_3O_4$/MWCNTs (c) catalysts in 0.5 M NaOH solution saturated by $N_2$ with scan rate of 50 mV $s^{-1}$.

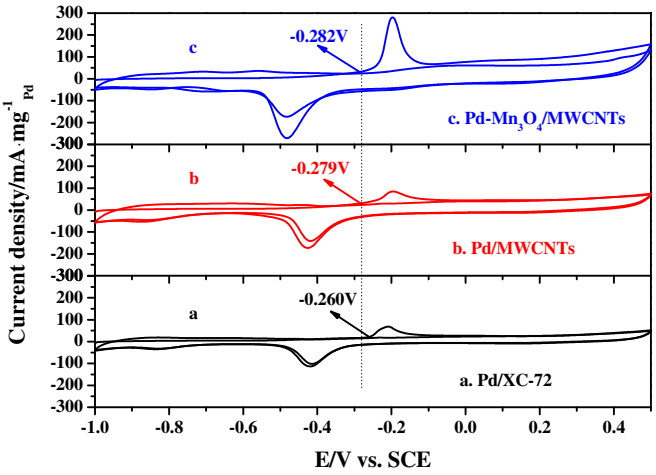


**Fig. 9.** CO-stripping voltammograms of (a) Pd/XC-72, (b) Pd/MWCNT, and (c) Pd–$Mn_3O_4$/MWCNT catalysts in 0.5 M NaOH at room temperature and 50 mV $s^{-1}$ scan rate.

with Pd–$Mn_3O_4$/MWCNT (Fig. 9c) catalysts in 0.5 M NaOH at a scan rate of 50 mV $s^{-1}$, respectively. All the parameters of CO stripping voltammograms are presented in Table 1. It can be seen that the hydrogen desorption peaks of all the catalysts in the first scan are largely suppressed in the lower potential region due to the saturation of the Pd surface with $CO_{ads}$ species. The CV curves show a single oxidation peak at $E \approx -0.2$ V, whereas no CO oxidation is monitored in the second scan, by which proves the complete removal of $CO_{ads}$ species. The onset potential of CO oxidation is observed at −0.26 V on Pd/XC-72, −0.279 V on Pd/MWCNTs and −0.282 V on Pd–$Mn_3O_4$/MWCNTs, suggesting the CO oxidation on Pd–$Mn_3O_4$/MWCNTs could proceed at slightly lower potential, indicating Pd–$Mn_3O_4$/MWCNTs catalyst has a higher CO oxidation ability [48]. Furthermore, a charge to metal area conversion factor of 420 μC $cm^{-2}$ for Pd is adopted to compute *ESA* of the catalysts [49]:

$$ESA = \frac{Q_{CO}}{420\ \mu C \cdot cm^{-2}}$$

Where $Q_{CO}$ is the charge for CO desorption electro-oxidation in microcoulomb (μC). The $Q_{CO}$ of the three catalysts is in the order of Pd–$Mn_3O_4$/MWCNTs (320 C $g^{-1}_{Pd}$) > Pd/MWCNTs (120 C $g^{-1}_{Pd}$) > Pd/XC-72 (80 C $g^{-1}_{Pd}$). All of these suggest that the presence of $Mn_3O_4$ can improve the activity of Pd/MWCNTs for CO electro-oxidation. The *ESA* for Pd–$Mn_3O_4$/MWCNTs (76.19 $m^2$ $g^{-1}$) is apparently higher than that of Pd/MWCNTs (28.57 $m^2$ $g^{-1}$) and Pd/XC-72 (19.05 $m^2$ $g^{-1}$). Pd–$Mn_3O_4$/MWCNT catalyst possesses larger *ESA* and is able to oxidize CO at lower potential, so it has less opportunity of being poisoned by $CO_{ads}$ species during the oxidation of methanol. The reason may be the smaller size and much better dispersion of the Pd nanoparticles on $Mn_3O_4$ modified MWCNTs (in Table 1). This also demonstrated that the Pd nanoparticles deposited on $Mn_3O_4$/MWCNTs are electrochemically more accessible, which is very important for electrocatalyst applications in fuel cells.

**Table 1**
Values of CO stripping performances at different catalysts.

| Electrocatalyst | ESA ($m^2$ $g^{-1}$) | $E_m$ (V) | $E_n$ (V) | $Q_{co}$ (C $g^{-1}_{Pd}$) |
|---|---|---|---|---|
| Pd–$Mn_3O_4$/MWCNTs | 76.19 | −0.282 | −0.197 | 320 |
| Pd/MWCNTs | 28.57 | −0.279 | −0.195 | 120 |
| Pd/XC-72 | 19.05 | −0.260 | −0.207 | 80 |

Electrochemical active surface area (ESA) obtained by CO-stripping Cyclic voltammogram, The onset potential ($E_m$) of electro-oxidation of pre-adsorbed CO; The peak potential ($E_n$) of electro-oxidation of pre-adsorbed CO peak potential, for different catalysts in 0.5 M NaOH solution at a sweep rate of 50 mV $s^{-1}$.

### 3.4. Evaluation of methanol electro-oxidation

The high *ESA* for Pd–$Mn_3O_4$/MWCNTs is also supported by the high electrocatalytic activity for the electro-oxidation reaction of methanol (Fig. 10A). The faradic current for the reaction exhibits the well-known features of methanol oxidation on Pd-based electrocatalysts in 0.5 M NaOH + 1.0 M $CH_3OH$ solution. A typical methanol oxidation peak in the forward scan can be clearly observed on all the electrocatalysts and the backward oxidation current peak can also be observed corresponding to the removal of the residual carbon species formed in the forward scan [50,51]. The electrochemical parameters for the methanol oxidation reaction including the onset potential ($E_s$), the forward anodic peak current densities ($j_p$) at $E_p$, the ratio of the forward anodic peak current ($I_f$) to the backward anodic peak current ($I_b$) are given in Table 2. It can be seen from Fig. 10A that Es of methanol oxidation peak of Pd–$Mn_3O_4$/MWCNTs shifts more than 160 mV toward negative potential as compared to that of Pd/MWCNTs. This indicates that the Pd–$Mn_3O_4$/MWCNT catalyst is able to reduce the overpotential significantly in methanol oxidation [52,53]. Furthermore, as

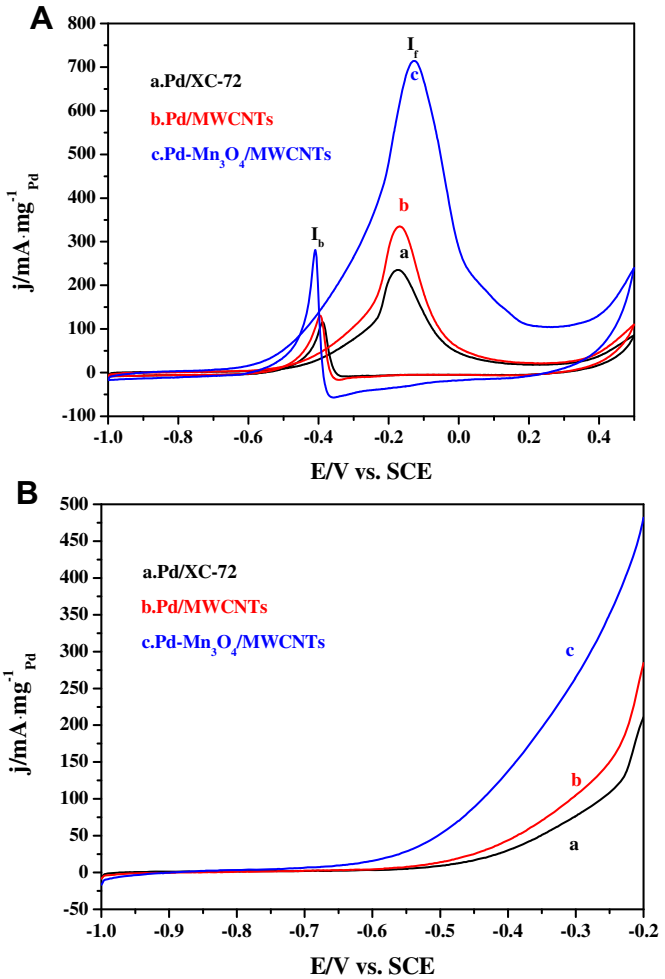


**Fig. 10.** Cyclic voltammograms (A) and linear sweep voltammetry (B) of the Pd/XC-72 (a), Pd/MWCNT (b) and Pd–$Mn_3O_4$/MWCNT (c) catalysts in 0.5 M NaOH + 1.0 M $CH_3OH$ solution saturated by $N_2$ with scan rate of 50 mV $s^{-1}$.

**Table 2**
Parameters of the methanol electro-oxidation reaction performances at different catalysts.

| Electrocatalyst | $E_s$ (V) | $j_p$ (mA $mg^{-1}_{Pd}$) | $I_f/I_b$ |
|---|---|---|---|
| Pd–$Mn_3O_4$/MWCNTs | −0.69 | 715.8 | 2.60 |
| Pd/MWCNTs | −0.53 | 332.4 | 2.50 |
| Pd/XC-72 | −0.51 | 236.1 | 2.04 |

Onset potential($E_s$), Forward Peak current ($j_p$) and Peak ratio($I_f/I_b$) of Pd/XC-72, Pd/MWCNT and Pd–$Mn_3O_4$/MWCNT electrocatalysts for $CH_3OH$ oxidation reaction in 0.5 M NaOH solution containing 1.0 M $CH_3OH$ at a sweep rate of 50 mV $s^{-1}$.

indicated in Fig. 10B, the corresponding potential on Pd–$Mn_3O_4$/MWCNTs is much lower than the others at a given oxidation current density. It means that Pd–$Mn_3O_4$/MWCNTs owns better performance for methanol electro-oxidation at all applied potentials (from −1.0 to −0.2 V) [54]. The Es of methanol oxidation reaction shifts negatively on the Pd–$Mn_3O_4$/MWCNT electrocatalysts, indicating the improvement in the reaction kinetics [15]. The methanol forward oxidation mass specific peak current of Pd–$Mn_3O_4$/MWCNTs (715.8 mA $mg^{-1}_{Pd}$) is 115.3% higher than that of the Pd/MWCNTs (332.4 mA $mg^{-1}_{Pd}$) and 203.1% higher than Pd/XC-72 (236.1 mA $mg^{-1}_{Pd}$). The prominently higher anodic current for the methanol oxidation on Pd–$Mn_3O_4$/MWCNT catalysts shows $Mn_3O_4$ plays a key role in the catalytic performance. Very likely, $Mn_3O_4$ nanoparticles act as a catalytic-activity-modifier and provide a suitable environment for the formation of Pd nanoparticles [55] and the oxidation of methanol. The higher electrocatalytic activity of Pd–$Mn_3O_4$/MWCNTs once again proves the importance of the distribution and dispersion of Pd nanoparticles on $Mn_3O_4$-MWCNT supports, in agreement with their small particles size and large surface.

In addition, it is well known that the ratio of $I_f/I_b$ is a useful index of the catalyst tolerance to incompletely oxidized species accumulated on the surface of the electrode. A higher ratio indicates more efficient removal of the poisoning species on the catalyst surface [31]. The $I_f/I_b$ ratio of Pd–$Mn_3O_4$/MWCNTs is about 2.60, which is higher than Pd/MWCNT (2.50) and Pd/XC-72 (2.04).

Fig. 11 shows Cyclic voltammograms of Pd/MWCNT (A) and Pd–$Mn_3O_4$/MWCNT (B) in 0.5 M NaOH + 1.0 M $CH_3OH$ electrolyte at different temperature. The reproducibility of the onset oxidation potential of $CH_3OH$, as well as the magnitude of the current, was low for both catalysts, which attributed to the fact that poisonous intermediates, such as CO, adsorbing to the electrode surface at low potentials, poison the electrode and alter the surface nature [56]. As the temperature of the fuel and electrolyte were increased, the currents increased, and the onset of oxidation is consistently observed at more negative potentials, indicating the electrocatalyst activity of this catalyst get better with temperature increasing. From Fig. 11A and B, it can be seen that the peak potential, $E_p$, for $CH_3OH$ oxidant (and concomitant oxide reduction) shifted to more positive potentials when the temperature was increased. This larger potential shift can be attributed to enhanced surface oxide consumption.

The apparent activation energy ($E_a$) has been calculated in many of similar temperature-dependent $CH_3OH$ oxidation studies [56]. These values are simply obtained by plotting ln (current density) as a function of 1/T at a given potential using the Arrhenius equation [56,57].

$$j = Ae^{-E_a/RT}$$

$$\ln j = \text{const.} - E_a/RT$$

Where j is the current density at a specific potential, $R$ is the gas constant, $T$ is the temperature in K, and $E_a$ is the apparent activation energy at a given potential. Fig. 11C shows representative Arrhenius plots for the Pd–$Mn_3O_4$/MWCNTs (a) and Pd/MWCNTs (b) in 0.5 M NaOH + 1.0 M $CH_3OH$ by sweeping anodically at −150 mV, respectively. The slope, intercept, and $R$ values of the linear fits are displayed on each curve. It can be seen that the slope of Pd–$Mn_3O_4$/MWCNT is smaller than that of Pd/MWCNT electrocatalysts. By fitting linear relationships between lnj and 1/T, it can be obtained

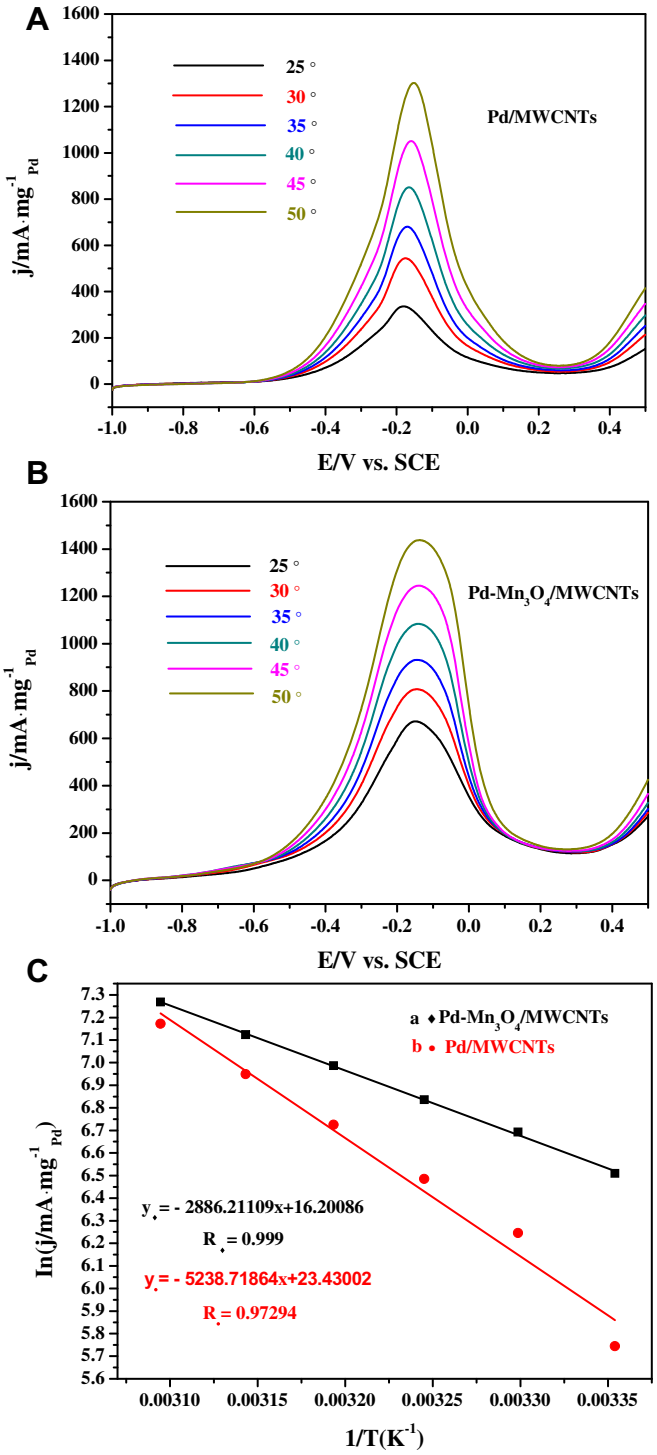


**Fig. 11.** LSV curves in 0.5 M NaOH + 1.0 M $CH_3OH$ solution at different temperatures for Pd/MWCNTs (A) Pd–$Mn_3O_4$/MWCNTs (B) and Arrhenius plots (C) For the Pd–$Mn_3O_4$/MWCNTs(◆) (a) and Pd/MWCNTs(•) (b) In 0.5 M NaOH + 1.0 M $CH_3OH$ for LSV carried out by sweeping anodically at −150 mV.

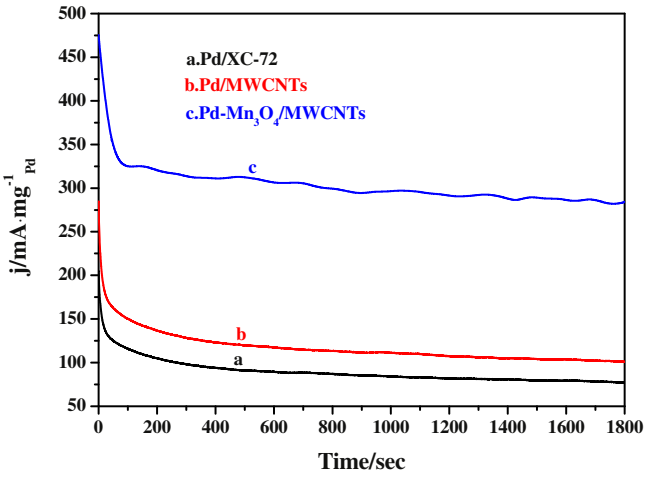


**Fig. 12.** Chronoamperometry of the Pd/XC-72 (a), Pd/MWCNT (b), and Pd–$Mn_3O_4$/MWCNT (c) catalysts collected for 1800 s at −0.2 V in 0.5 M NaOH + 1.0 M $CH_3OH$ solution saturated by $N_2$ at room temperature.

that the $E_a$ for Pd/MWCNTs and Pd–$Mn_3O_4$/MWCNTs are 43.56 and 23.99 kJ $mol^{-1}$, respectively. The smaller $E_a$ of Pd–$Mn_3O_4$/MWCNTs demonstrates that methanol electro-oxidation on Pd–$Mn_3O_4$/MWCNTs is easier than Pd/MWCNT catalysts [57].

Chronoamperometric technique is an effective method to evaluate the electrocatalytic activity and stability of catalyst materials. In order to compare the long-term performance of the three catalysts, we also conducted chronoamperometry tests in a solution of 0.5 M NaOH + 1.0 M $CH_3OH$ for 1800 s Fig. 12 shows the chronoamperometric curves for the Pd/XC-72 (a), Pd/MWCNT (b) and Pd–$Mn_3O_4$/MWCNT (c) electrodes at a potential of −0.2 V. From Fig. 12, we can see that all of catalysts present a gradual current decay before a steady current status was attained, which was attributed to the formation of some Pd and Mn oxides/hydroxides and adsorbed to intermediates in methanol electro-oxidation reaction. The rendered current density values for methanol oxidation on Pd–$Mn_3O_4$/MWCNT, Pd/MWCNT and Pd/XC-72 electrocatalysts measured after 1800 s were 284.14 (decreased by 40.23% compared with initial current density), 101.03 (64.38%) and 77.25 mA $mg^{-1}$ Pd (62.19%), respectively. These results indicate that the Pd–$Mn_3O_4$/MWCNT electrocatalyst has the best electrocatalytic stability and poisoning tolerance among three catalysts in alkaline medium.

## 4. Conclusions

A novel Pd–$Mn_3O_4$/MWCNT composite was prepared by a facile method at room temperature without any expensive chemicals or rigorous condition. $Mn_3O_4$ nanocrystals homogeneously attached on the exteriors of MWCNTs provided active sites for deposition of Pd nanoparticles. Meantime, the presence of $Mn_3O_4$ improved catalytic activity of composites significantly, owing to the formation of MnOOH, $Mn_2O_3$ and $MnO_2$ species during the electrode reaction process. Compared with Pd/MWCNT and Pd/XC-72, Pd–$Mn_3O_4$/MWCNT composites have the largest electrochemical active surface area and endurance of poisoned by $CO_{ads}$ species. The excellent catalytic performance of Pd–$Mn_3O_4$/MWCNTs for methanol oxidation suggests it be a promising candidate for portable applications in alkaline direct methanol fuel cells.

## Acknowledgments

This work has been supported by the National Natural Science Foundation of China (No. 21163002, 21165004), Guangxi Natural Science Foundation of China (2010GXNSFF013001, 0728043), the project of Key Laboratory for the Chemistry and Molecular Engineering of Medicinal Resources (Guangxi Normal University), Ministry of Education of China(CMEMR2011-14) and Innovation Plan in Graduate Education of Guangxi Province (2011106020703M48).

## References

[1] J. Park, E. Kang, C.J. Bae, J.G. Park, H.J. Noh, J.Y. Kim, J.H. Park, H.M. Park, Taeghwan Hyeon*, J. Phys. Chem. B 108 (2004) 13594–13598.
[2] Y. Zhao, C. Li, F. Li, Z. Shi, S. Feng, Dalton Trans. 40 (2011) 583–588.
[3] G. Salazar-Alvarez, J. Sort, S. Suriñach, M.D. Baró, J. Nogués, J. Am. Chem. Soc. 129 (2007) 9102–9108.
[4] O. Giraldo, S.L. Brock, W.S. Willis, M. Marquez, S.L. Suib, S. Ching, J. Am. Chem. Soc. 122 (2000) 9330–9331.
[5] J.M. Tarascon, M. Armand, Nature 414 (2001) 359–367.
[6] E.R. Stobbe, B.A.D. Boer, J.W. Geus, Catal. Today 47 (1999) 161–167.
[7] E.J. Grootendorst, Y. Verbeek, V. Ponec, J. Catal. 157 (1995) 706–712.
[8] H. Wang, L.-F. Cui, Y. Yang, H.S. Casalongue, J.T. Robinson, Y. Liang, Y. Cui, H. Dai, J. Am. Chem. Soc. 132 (2010) 13978–13980.
[9] P.K. Shen, C. Xu, Electrochem. Commun. 8 (2006) 184–188.
[10] M.-W. Xu, G.-Y. Gao, W.-J. Zhou, K.-F. Zhang, H.-L. Li, J. Power Sources 175 (2008) 217–220.
[11] B. Messaoudi, S. Joiret, M. Keddam, H. Takenouti, Electrochim. Acta 46 (2001) 2487–2498.
[12] Innocenzo G. Casella, J. Electroanal. Chem. 520 (2002) 119–125.
[13] D. Zhang, D. Chi, T. Okajima, T. Ohsaka, Electrochim. Acta 52 (2007) 5400–5406.
[14] S.-E. Chun, S.-I. Pyun, G.-J. Lee, Electrochim. Acta 51 (2006) 6479–6486.
[15] C. Xu, Z. Tian, P. Shen, S. Jiang, Electrochim. Acta 53 (2008) 2610–2618.
[16] C. Xu, P. Shen, Y. Liu, J. Power Sources 164 (2007) 527–531.
[17] K.F. Zhang, D.J. Guo, X. Liu, J. Li, H.L. Li, Z.X. Su, J. Power Sources 162 (2006) 1077–1081.
[18] Y.-G. Wang, L. Cheng, F. Li, H.-M. Xiong, Y.-Y. Xia, Chem. Mater. 19 (2007) 2095–2101.
[19] A. Vazquezolmos, R. Redon, G. Rodriguezgattorno, M. Esthermatazamora, F. Moralesleal, A. Fernandezosorio, J. Saniger, J. Colloid Interface Sci. 291 (2005) 175–180.
[20] W.S. Kijlstra, J.C.M.L. Daamen, J.M.V.D. Graaf, B.V.D. Linden, E.K. Poels, A. Bliek, Appl. Catal. B 7 (1996) 337–357.
[21] E. Mendelovici, A. Sagarzazu, Thermochim. Acta 133 (1988) 93–100.
[22] E. Finocchio*, G. Busca, Catal. Today 70 (2001) 213–225.
[23] F. Davar, M. Salavati-Niasari, N. Mir, K. Saberyan, M. Monemzadeh, E. Ahmadi, Polyhedron 29 (2010) 1747–1753.
[24] X. Zhong, R. Xie, L. Sun, I. Lieberwirth, W. Knoll, J. Phys. Chem. B 110 (2006) 2–4.
[25] X. Dong, W. Shen, J. Gu, L. Xiong, Y. Zhu, H. Li, J. Shi, J. Phys. Chem. B 110 (2006) 6015–6019.
[26] Aditi Halder, Sudhanshu Sharma, M.S. Hegde, N. Ravishankar, J. Phys. Chem. C 113 (2009) 1466–1473.
[27] G. An, P. Yu, M. Xiao, Z. Liu, Z. Miao, K. Ding, L. Mao, Nanotechnology 19 (2008) 275709–275715.
[28] Y.C. Zhao, L. Zhan, J.N. Tian, S.L. Nie, Z. Ning, Int. J. Hydrogen Energy 35 (2010) 10522–10526.
[29] M. Salavati-Niasari, F. Davar, M. Mazaheri, Polyhedron 27 (2008) 3467–3471.
[30] S. Apte, S. Naik, R. Sonawane, B. Kale, N. Pavaskar, A. Mandale, B. Das, Mater. Res. Bull. 41 (2006) 647–654.
[31] Y.C. Zhao, X.L. Yang, J.N. Tian, F.Y. Wang, L. Zhan, Int. J. Hydrogen Energy 35 (2010) 3249–3257.
[32] A.K. Datye, J. Bravo, T.R. Nelson, P. Atanasova, M. Lyubovsky, L. Pfefferle, Appl. Catal. A 198 (2000) 179–196.
[33] M. Wang, W. Liu, C. Huang, Int. J. Hydrogen Energy 34 (2009) 2758–2764.
[34] J. Prabhuram, T.S. Zhao, Z.K. Tang, R. Chen, Z.X. Liang, J. Phys. Chem. B 110 (2006) 5245–5252.
[35] G. Guo, F. Qin, D. Yang, C. Wang, H. Xu, S. Yang, Chem. Mater. 20 (2008) 2291–2297.
[36] F. Cheng, H. Wang, Z. Sun, M. Ning, Z. Cai, M. Zhang, Electrochem. Commun. 10 (2008) 798–801.
[37] H. Xu, S. Xu, X. Li, H. Wang, H. Yan, Appl. Surf. Sci. 252 (2006) 4091–4096.
[38] F. Buciuman, F. Patcas, R. Craciun, D.R.T. Zahn, Phys. Chem. Chem. Phys. 1 (1999) 185–190.
[39] C.-C. Hu, Y.-T. Wu, K.-H. Chang, Chem. Mater. 20 (2008) 2890–2894.
[40] N. Yao, V. Lordi, S.X.C. Ma, E. Dujardin, A. Krishnan, M.M.J. Treacy, T.W. Ebbesen, J. Mater. Res. 13 (1998) 2432–2437.
[41] Y.C. Zhao, X.L. Yang, J.N. Tian, F.Y. Wang, L. Zhan, J. Power Sources 195 (2010) 4634–4640.
[42] S. Wang, X. Wang, S.P. Jiang, Langmuir 24 (2008) 10505–10512.
[43] J. Li, Y. Liang, Q. Liao, X. Zhu, X. Tian, Electrochim. Acta 54 (2009) 1277–1285.
[44] Y.C. Zhao, X.L. Yang, J.N. Tian, Electrochim. Acta 54 (2009) 7114–7120.
[45] R. Singh, A. Singh, Anindita, Carbon 47 (2009) 271–278.
[46] Y.C. Zhao, X.L. Yang, J.N. Tian, F.Y. Wang, L. Zhan, Mater. Sci. Eng. B 171 (2010) 109–115.

[47] R.N. Singh, A. Singh, Anindita, Int. J. Hydrogen Energy 34 (2009) 2052–2057.
[48] Y.C. Zhao, F.Y. Wang, J.N. Tian, X.L. Yang, L. Zhan, Electrochim. Acta 55 (2010) 8998–9003.
[49] T. Vidakovic, M. Christov, K. Sundmacher, Electrochim. Acta 52 (2007) 5606–5613.
[50] Z. Liu, X. Zhang, L. Hong, Electrochem. Commun. 11 (2009) 925–928.
[51] Z.P. Sun, X.G. Zhang, R.L. Liu, Y.Y. Liang, H.L. Li, J. Power Sources 185 (2008) 801–806.
[52] Z.Z. Zhu, Z. Wang, H.L. Li, J. Power Sources 186 (2009) 339–343.
[53] D.-J. Guo, L. Zhao, X.-P. Qiu, L.-Q. Chen, W.-T. Zhu, J. Power Sources 177 (2008) 334–338.
[54] J.-J. Shi, G.-H. Yang, J.-J. Zhu, J. Mater. Chem. 21 (2011) 7343–7349.
[55] X. Gong, Y. Yang, S. Huang, Chem. Commun. 47 (2011) 1009–1011.
[56] J.L. Cohen, D.J. Volpe, H.D. Abruna, Phys. Chem. Chem. Phys. 9 (2007) 49–77.
[57] Y. Wang, X. Wang, C.M. Li, Appl. Catal. B: Environ. 99 (2010) 229–234.